

LETTER

Extended UV detection bandwidth: h-BN/Al powder nanocomposites photodetectors sensitive in a middle UV region due to localized surface plasmon resonance effect


To cite this article: Ilia N. Volkov *et al* 2021 *EPL* **133** 28002

View the [article online](#) for updates and enhancements.

You may also like

- [Non-chemical fluorination of hexagonal boron nitride by high-energy ion irradiation](#)
Shiro Entani, Konstantin V Larionov, Zakhar I Popov et al.
- [Coating performance of hexagonal boron nitride and graphene layers](#)
Xuemei Li, Yuyang Long, Limin Ma et al.
- [Dependence of the polycarbonate mechanical performances on boron nitride flakes morphology](#)
Emanuele Lago, Peter S Toth, Silvia Gentiluomo et al.

Extended UV detection bandwidth: h-BN/Al powder nanocomposites photodetectors sensitive in a middle UV region due to localized surface plasmon resonance effect

ILIA N. VOLKOV^{1(a)} , ZHANNA S. YERMEKOVA¹, ALMAZ I. KHABIBRAKHMANOV¹, ANDREY M. KOVALSKI¹, SHAKTY CORTHEY¹, ALEXEY R. TAMEEV², ALEXEY E. ALEKSANDROV², PAVEL B. SOROKIN¹, DMITRY V. SHTANSKY¹ and ANDREI T. MATVEEV¹

¹ National University of Science and Technology “MISIS” - Leninsky Prospect 4, Moscow, 119049, Russian Federation

² A.N. Frumkin Institute of Physical Chemistry and Electrochemistry, Russian Academy of Sciences
Leninsky Prospect 31, bld.4, Moscow, 119071, Russian Federation

received 5 October 2020; accepted in final form 11 December 2020

published online 22 March 2021

PACS 85.60.Gz – Photodetectors (including infrared and CCD detectors)

PACS 73.20.Mf – Collective excitations (including excitons, polarons, plasmons and other charge-density excitations)

PACS 78.67.Sc – Nanoaggregates; nanocomposites

Abstract – The development of high-effective photodetectors operating in a wide spectral range is an important technological task. In this work we have demonstrated that the detection bandwidth of *h*-BN photodetectors in the UV range can be extended due to the surface plasmon resonance (SPR) effect. Theoretical calculations showed that, among Al, Au, Ag, and Cu, Al is the most suitable metal for the *h*-BN UV sensible detectors due to the SPR effect in the middle UV range. Based on the theoretical predictions, a simple and highly efficient method for obtaining *h*-BN/Al nanocomposites for localized SPR-based UV detectors was developed. It was demonstrated that the *h*-BN/Al material is sensitive to UV radiation with a wavelength of 266 nm that is far away of the detection limit of 240 nm inherent for pure *h*-BN.

Copyright © 2021 EPLA

Exploration and design of plasmon active materials are indispensable to explore, design, and build nanophotonic devices [1].

Monitoring and acquisition of information on the UV radiation in a 200–280 nm region is an important aspect for the environmental and medical research, studies of optical phenomena, and various industrial applications [2–4]. The following materials are most commonly used as UV detector components: Ga₂O₃ [5], SnO₂ [6,7], WO₃ [8], ZnO [9–11], Si [12–14], SiC [15], AlN [16,17], GaN [13,18,19], GaO [20], perovskites [21], diamond [22] and TiO₂ [23]. The hexagonal boron nitride (*h*-BN) is widely utilized in optoelectronics [24–26] due to its unique physical properties, high chemical and thermal stability, and insulating nature. Due to the wide bandgap (~6 eV), the *h*-BN is a promising material for solar blind detectors operating in a far UV region [27–30], and the

best performance of photonic cell was reported for a thin *h*-BN active layer [31–33]. A photodetector consisting of a few atomic layers *h*-BN film produced by ion beam assisted deposition (IBSD) exhibited an on/off ratio of >10³ under illumination at 212 nm wavelength and the cutoff wavelength at around 225 nm [32]. Carbon-doped *h*-BN atomic layers prepared by IBSD and wet-transfer method were also demonstrated to be a promising material for high-performance far UV photodetectors [33]. Their cutoff wavelength was about 226 nm. The largest cutoff wavelength of approximately 250 nm was reported for a photodetector made of pulsed laser deposited *h*-BN nanosheets containing a significant amount of boron oxide [31]. Thus, an urgent and highly demanded task is to expand the detection range of far UV radiation and to develop a simple and reproducible technology for manufacturing such detectors.

The surface modification can significantly improve performance of photodetectors. In particular, the

^(a)E-mail: ilia.volkov@outlook.com

optoelectronic properties of photonic detectors can be increased by the surface plasmon resonance (LSPR) effect [34–40]. The mechanism of the effect can be in general described as following. Under the incident electromagnetic radiation (light) collective oscillations of conduction electrons in metals can be excited. The quanta of these oscillations are called plasmons. At the specific light frequency, depending on electron concentration and their effective mass in metal, these oscillations may become resonant. The corresponding frequency is called plasmonic resonance frequency, and the effect is called surface plasmon resonance (SPR) because at the plasmon frequency plasmons are excited in a thin surface layer. In metallic nanoparticles SPR is called localized SPR (LSPR), because plasmons' habitat is limited by the nanoparticle. Besides, plasmons can be localized by tip-shaped surface perturbations of metallic nanoparticles, and in this case they are called superlocalized plasmons [41]. Nanoparticles of Au, Pt, and Ag are widely studied as the plasmonic nanoantennas because of strong SPR effect in these metals. Mono- and bi-metallic NPs exhibit the dynamic LSPR peaks in the visible region (450–700 nm) based on their morphology and elemental composition [42]. Electron transfer from Au NPs to ZnO quantum dots (QDs) mediated by LSPR leads to the decrease of visible-range emission and the increase of UV-range emission [10]. Unlike noble metals, aluminum possesses a much shorter absorption wavelength of ~ 143 nm [43]. Therefore, the use of aluminum for plasmonic nanostructures opens up new possibilities, such as access to short-wavelength regions of the spectrum, complementary metal-oxide-semiconductor (CMOS) compatibility, and the possibility of low-cost, sustainable, mass-producible plasmonic materials [44].

The sensitivity of up-to-date *h*-BN-based photodetectors is below 240 nm because of insufficient photon energy to excite localized electrons to enter the conduction band [16,40,45–49]. This limitation can be overcome by local enhancement of electromagnetic field strength in a thin *h*-BN layer caused by the surface plasmon resonance (SPR) effect in metal in the vicinity of *h*-BN. Regarding photoconductivity, two major processes of energy redistribution of excited plasmons have been proposed [50]: i) direct transfer of electrons from the metal nanoparticles to the conduction band of the semiconductor upon electron resonance energy absorption of incident photons; ii) the LSPR-powered bandgap breaking effect. The former process is also called the “LSPR sensitization effect” because of similarities with the sensitization of TiO₂ by organic dyes. This process was suggested to explain direct transfer of electrons from Au nanoparticles to TiO₂ mediated by LSPR under irradiation with visible light [51] and even with near-infrared light [52]. The latter process requires the energy of the surface plasmon to be equal to or larger than the bandgap of the semiconductor. Upon LSPR an enhancement factor $|E|^2/E_0^2$ of the local electric field amplitude $|E|$ to the original electric field $|E_0|$ of the light for single nanoparticles can reach values of

10–100 [53–55], but in the case of nanoparticle aggregates field enhancement of at least one order of magnitude larger can be achieved [54,56]. Based on a combination of the enhanced near-surface electric field by the LSPR and the “hot electron” injection process the photoresponse of ZnO/Au heterostructures photodetectors was effectively extended to the visible range with a remarkably improved photoresponse [55].

The SPR effect was evaluated based on the extinction section (C_{ext}) of metal spheres and was compared for several metals (Al, Au, Ag, and Cu). The details of theoretical approaches for assessing this quantity could be found elsewhere [57]. Here the calculations were carried out according to the equation for the simplified case of a spherical nanoparticle placed inside the dielectric material [58] (fig. 1 in the Supplementary Material [Supplementarymaterial.pdf](#) (SM)):

$$C_{ext} = 9 \frac{\omega}{c} \varepsilon_m^{3/2} V \frac{\varepsilon_2(\omega)}{[\varepsilon_1(\omega) + 2\varepsilon_m]^2 + \varepsilon_2^2(\omega)}, \quad (1)$$

where C_{ext} and V are the extinction cross-section and volume of metal spheres, ω is the frequency of electromagnetic radiation, c is the speed of light in a vacuum, ε_m is the dielectric permittivity of the dielectric medium (*h*-BN in the case under consideration), $\varepsilon = \varepsilon_1 + i\varepsilon_2$ is the dielectric function of the metal which depends on the incident radiation frequency. The C_{ext} is the sum of cross-sections for scattering and absorption of light by metal spheres. The real part of the metal dielectric function is negative in case of frequencies lower than the plasma frequency. Therefore, this may lead to the resonance increase of the C_{ext} value under the $\varepsilon_1(\omega_0) = -2\varepsilon_m$ condition. The ω_0 frequency in this case is called the SPR frequency [58].

According to eq. (1), the SPR frequency is also influenced by dielectric permittivity ε_m . We calculated ε_m based on the density functional theory (DFT) [59] with generalized gradient approximation (GGA) in the Perdew-Burke-Ernzerhof (PBE) parametrization [60] using the Vienna *Ab initio* Simulation Package (VASP) software [61]. *h*-BN was modelled as a hexagonal layered structure with AA' layer stacking. Grimme's van der Waals correction [62] was used to describe the interlayer distance. The lattice parameters obtained after both ions and cell relaxation were $a = 2.51$ Å and $c = 6.17$ Å. The dielectric tensor was calculated in VASP using the density functional perturbation theory (DFPT) as described elsewhere [63]. In *h*-BN, there are only 2 independent dielectric constants: in-plane $\varepsilon_{||} = 5.0$ and out-of-plane $\varepsilon_{\perp} = 3.1$ (in the units of $\varepsilon_0 = 8.85 \cdot 10^{-12}$ F/m). The obtained results for *h*-BN lattice constants and dielectric constants are in good agreement with the previous data [64]. For simplicity, we take ε_m in eq. (1) equal to the trace of the dielectric tensor: $\varepsilon_m = (2\varepsilon_{||} + \varepsilon_{\perp})/3 = 4.4$. For Cu, Au, Ag, and Al metals, the experimental dielectric function $\varepsilon(\omega)$ was used [65,66].

The extinction section calculated according to eq. (1) for various metals is depicted in fig. 1. One can see that resonant frequencies for Cu, Ag, and Au are in the visible

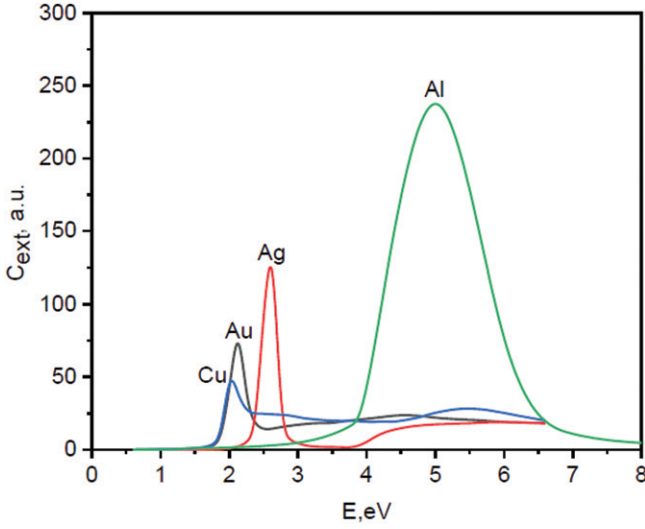


Fig. 1: Extinction cross-section of various metal spheres calculated from eq. (1) and plotted as a function of incident photon energy.

range (between 2 and 3 eV), whereas in the case of the Al particle, $\omega_0 \approx 5$ eV (248 nm) that is in the UV range. The Al LSPR peak width corresponds to 210–310 nm wavelength range and Al particles lead to the highest C_{ext} peak. Al nanoparticles are well known for their wide range of plasmon tunability (200–700 nm) [67], and they were successfully used before for modification of photodevices by means of LSPR [68,69]. The reported LSPR peak wavelengths 294 nm [68] and 269 nm [69] are in good agreement with our obtained results. The difference could be attributed to the different substrates: as follows from eq. (1), with the increase of the substrate dielectric permittivity the resonant frequency ω_0 redshifts. Therefore, the results presented in fig. 1 indicate that Al has a maximum potential as a plasmonic metal for the SPR-activated *h*-BN UV detector.

Guided by theoretical prediction we have manufactured the UV detector cell based on the *h*-BN/Al and *h*-BN/Au nanocomposites. Commercially available Al nanopowder of ~ 100 nm (RSS-NANO, Russia) and *h*-BN of ~ 10 –20 nm synthesized from ammonium borate hydrate [70] were used as powder precursors. Three mixtures *h*-BN:Al with a weight ratio of 2:1, 1:1, and 1:2 were subjected to HEBM at a speed of 800 rpm for 20 min using a Emax (Retsch GmbH, Germany) ball miller with the ZrO_2 jars and balls (diameter 10 mm). To prevent the milled nanomaterials from oxidation, processing was carried out in an Ar atmosphere (99,998%, PGS-service, Russia). A mixture *h*-BN/Au composite with the weight ratio of 2:1 and an average size of Au nanoparticles of ~ 20 nm was prepared by a common citrate reduction method of $\text{HAuCl}_4 \cdot 3\text{H}_2\text{O}$ in a water suspension of *h*-BN nanopowder (fig. 2 in the SM).

According to the XRD analysis (Cr $K\alpha$ radiation, fig. 2(A)), Al (ICCD #02-1109) is the main crystalline phase in the composite after the ball milling stage. A tiny

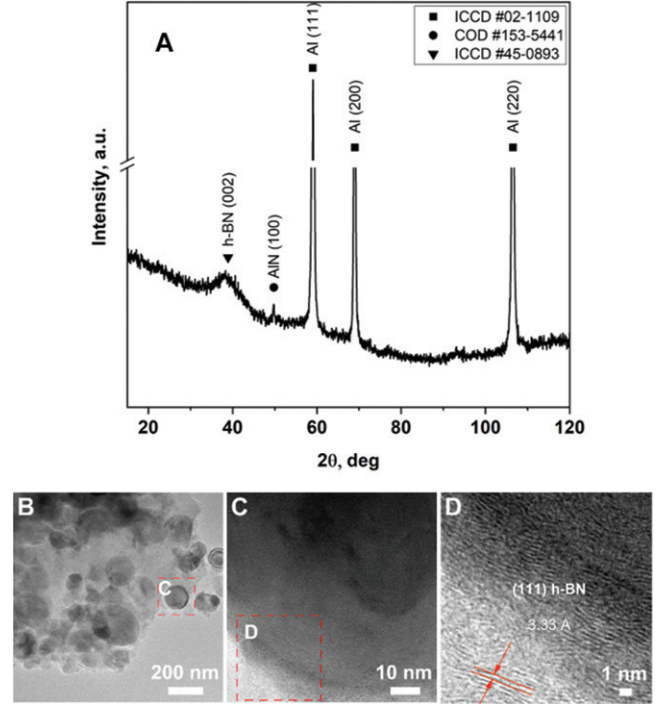


Fig. 2: (A) XRD pattern of *h*-BN/Al composite after HEBM (Cr $K\alpha$ radiation); (B)–(D) TEM images of the *h*-BN/Al composite after HEBM.

peak at $2\theta \sim 50^\circ$ can be attributed to the AlN phase (COD #153-5441). The *h*-BN peak at $2\theta \sim 40.24^\circ$ (ICCD #45-0893) is very broad and of low intensity indicating the highly defective structure of *h*-BN after the HEBM.

HR-TEM micrograph shows that Al nanoparticles preserved their initial shape and size (fig. 2(B)), whereas the *h*-BN appears as nanocrystals of a few nanometers well smeared all over the Al particle (fig. 2(C), (D)). As seen in fig. 2(C), each particle has a core/shell structure consisting of a ~ 100 nm Al core surrounded by a ~ 10 nm *h*-BN shell. This is almost an ideal structure for the localized SPR effect [71].

The photoconductivity of as-prepared *h*-BN/Al powder nanomaterials was measured on the UV detection cell shown in fig. 3. The *h*-BN/Al and *h*-BN/Au powders were pressed into pellets of 13 mm in diameter and ~ 1 mm in thickness in a die with a load of 10 tonn. Shaped pieces of the pellets were placed between a UV transparent quartz plate with deposited Nb electrodes and a silicone polymer dielectric strip. Two pairs of electrodes (4 mm length, 100 μm width with 5 μm distance between them) were used for the measurement on each sample.

The construction was tightly fixed between two holders to press the pellets to the electrodes.

A mercury lamp with the UV irradiation distributed between 4.1 eV and 6.1 eV (fig. 3 in the SM) was used in photoconductivity measurements; the UV incident power was calibrated with an irradiance Energy/Power Meter PE25-S (Ophir).

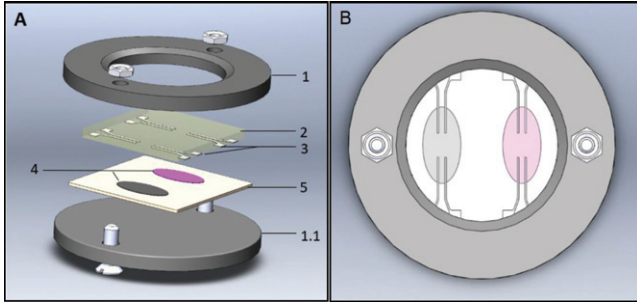


Fig. 3: Side (A) and top (B) view of the photonic cell. 1: upper holder with the open window; 1.1: bottom solid part of the metal holder; 2: UV transparent quartz plate; 3: sputtered Nb electrodes; 4: *h*-BN/Al and *h*-BN/Au pellets; 5: thin silicone strip.

For Al nanoparticles, a maximum of SPR located between approximately 4.0 eV and 6.2 eV (fig. 1) matches well with the used irradiation range of a Hg lamp. Due to this reason, *h*-BN/Al composites possess UV-induced photoconductivity in contrast to neat *h*-BN (table 1).

The photocurrent was measured at an applied voltage of 30 V with a Keithley 2400 source-meter unit. The instrument measurement error was below 10%. The *h*-BN/Al (2:1) composite exhibited the highest photoconductivity among the measured mixtures; decreasing photoresponse with Al concentration is probably associated with increasing shadow effect of the Al nanoparticles.

I-*V* curves measured on the *h*-BN/Al (2:1), and *h*-BN/Au composites and virgin *h*-BN under illumination of the Hg lamp are shown in fig. 4. Normalized photocurrent defined as $I_{\text{photo}}/I_{\text{dark}} \times 100\%$ is shown in the insert in fig. 4. It rises to almost 70% at 30 V. The responsivity of the *h*-BN/Al cell at this voltage reaches 40 $\mu\text{A}/\text{W}$.

These measurements have shown that the photocurrent of pure *h*-BN is in the range of nanoamperes, that well correlates with photoconductivity of thin *h*-BN films [72]. The *h*-BN/Au composite shows slightly higher conductivity, which is probably related to increase in total conductivity of the composite with addition of Au nanoparticles, but not to photoconductivity. Therefore, we consider that there is no photoresponse on the *h*-BN/Au composite in compliance with our theoretical calculations. Contrary, the *h*-BN/Al composite demonstrates steep elevation of conductivity under illumination.

Although only $\sim 10\%$ of the spectral energy density of the used Hg lamp accounts for the interval below 240 nm, *i.e.*, in the absorption range of *h*-BN (fig. 3 in the SM), nevertheless, to completely exclude an exciting effect from this shortwave spectrum range and to demonstrate the extended working wavelength of the *h*-BN/Al cell, it was irradiated by the 266 nm wavelength pulses (4th harmonic of a Nd-YAG laser). The laser pulse duration and energy were 10 ns (at the full-width-at-half-maximum) and 0.15 mJ, respectively. Using the 12,5 Hz pulse repetition rate, samples were irradiated for

Table 1: UV-induced photoconductivity of *h*-BN and *h*-BN/Al composites.

Weight ratio of <i>h</i> -BN:Al	Photocurrent, A		
	3 V	10 V	30 V
0	—	$<3.0 \times 10^{-11}$	$<3.0 \times 10^{-11}$
2:1	0.15×10^{-9}	0.4×10^{-9}	2.7×10^{-9}
1:1	—	0.3×10^{-10}	1.5×10^{-10}
1:2	—	$<3.0 \times 10^{-11}$	$<3.0 \times 10^{-11}$

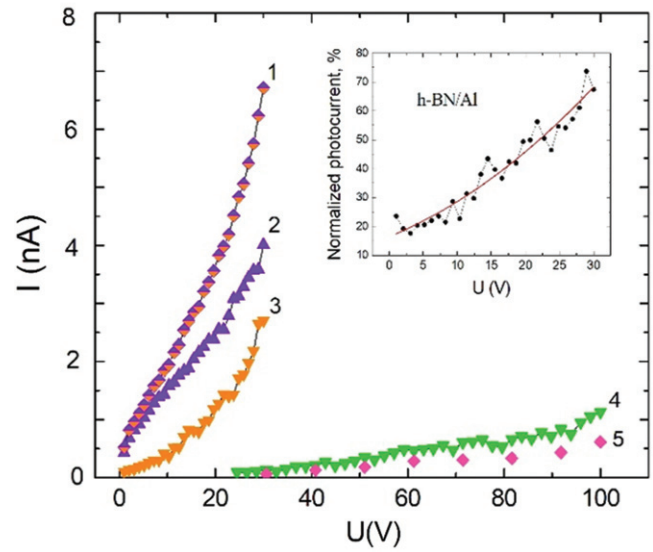


Fig. 4: *I*-*V* curves of the *h*-BN/Al (2:1) and *h*-BN/Au composites and virgin *h*-BN under middle-UV illumination. Curves 1, 2, and 3 show total current, dark current and photocurrent of the *h*-BN/Al composite, respectively; curve 4 shows the photocurrent of the *h*-BN/Au composite; symbols 5 refer to photocurrent of virgin *h*-BN. The insert shows the normalized photocurrent of the *h*-BN/Al cell.

30 seconds. The photocurrent was measured at an applied voltage of 200 V. An instrument measurement error was below 10%. The *h*-BN/Al composite had a dark current of 0.4 nA, which increased by 0.13 nA with laser irradiation, which is $\sim 33\%$ of the *h*-BN/Al nanohybrid without UV illumination. Responsivity of the cell reaches 0,1 mA/W.

Thus, we have successfully demonstrated that the nanocomposite composed of Al nanoparticles covered with a thin *h*-BN layer exhibited enhanced photocurrent in the range significantly beyond the detection limit of 240 nm inherent for pure *h*-BN. This effect was ascribed to AL-LSPR-mediated excitation of electrons in *h*-BN. The accurate mechanism of the excitation is not clear and requires additional research.

In conclusion, we would like to underline some important aspects of this work. Using the simplest model of SPR for a metal sphere placed inside a *h*-BN matrix we have calculated the light extinction cross-sections for Cu, Ag, Au, and Al metals. We found that Al is the plasmonic metal in UV range and therefore Al nanoparticles can be used for the localized SPR to enhance photosensitivity of *h*-BN in extended wavelength range determined by the *h*-BN band gap value. The theoretical prediction was successfully confirmed experimentally. Our results indicated that the application area of the UV *h*-BN-based detector can be extended to a longer wavelength of at least 266 nm, which has never been reported before. For the first time it was shown that a simple, highly scalable, and well reproducible HEBM powder technology approach can be utilized for the fabrication of a *h*-BN/Al UV sensible composite used as an active material for the photonic cell manufacturing.

INV thanks the Ministry of Education and Science of Russian Federation (Increase Competitiveness Program of NUST "MISIS" No. K2-2018-039).

Data availability statement: The data that support the findings of this study are available from the corresponding author upon reasonable request.

REFERENCES

- [1] LI Z.-Y., *EPL*, **110** (2015) 14001.
- [2] GUO D., GUO Q., CHEN Z., WU Z., LI P. and TANG W., *Mater. Today Phys.*, **11** (2019) 100157.
- [3] SABRI Y. M., KANDJANI A. E., RASHID S. S. A. A. H., HARRISON C. J., IPPOLITO S. J. and BHARGAVA S. K., *Sens. Actuators B: Chem.*, **275** (2018) 215.
- [4] MADHAIYAN G., TUNG T. W., ZAN H. W., MENG H. F., LU C. J., ANSARI A., CHUANG W. T. and LIN H. C., *Sens. Actuators B: Chem.*, **320** (2020) 128392.
- [5] QIAN L. X., LIU X. Z., SHENG T., ZHANG W. L., LI Y. R. and LAI P. T., *AIP Adv.*, **6** (2016) 045009.
- [6] CHEN D., WEI L., MENG L., WANG D., CHEN Y., TIAN Y., YAN S., MEI L. and JIAO J., *Nanoscale Res. Lett.*, **13** (2018) 92.
- [7] XIE T., HASAN M. R., QIU B., ARINZE E. S., NGUYEN N. V., MOTAYED A., THON S. M. and DEBNATH R., *Appl. Phys. Lett.*, **107** (2015) 241108.
- [8] HUO N., YANG S., WEI Z. and LI J., *J. Mater. Chem. C*, **1** (2013) 3999.
- [9] LU C. Y., CHANG S. J., CHANG S. P., LEE C. T., KUO C. F., CHANG H. M., CHIOU Y. Z., HSU C. L. and CHEN I. C., *Appl. Phys. Lett.*, **89** (2006) 153101.
- [10] FAN X., XU C., HAO X., TIAN Z. and LIN Y., *EPL*, **106** (2014) 67001.
- [11] HAN S., HU S. R., CAO P. J., LIU W. J., ZENG Y. X., JIA F., XU W. Y., LIU X. K., ZHU D. L. and LU Y. M., *EPL*, **124** (2018) 18006.
- [12] SOSNA-GLĘBSKA A., SIBIŃSKI M., SZCZECIŃSKA N. and APOSTOLUK A., *Mater. Today Proc.*, **20** (2020) 25.
- [13] ANITHA R., RAMESH R., LOGANATHAN R., VAVILAPALLI D. S., BASKAR K. and SINGH S., *Appl. Surf. Sci.*, **435** (2018) 1057.
- [14] YANG W., HU K., TENG F., WENG J., ZHANG Y. and FANG X., *Nano Lett.*, **18** (2018) 4697.
- [15] ALDALBAHI A., LI E., RIVERA M., VELAZQUEZ R., ALTALHI T., PENG X. and FENG P. X., *Sci. Rep.*, **6** (2016) 23457.
- [16] LI J., MAJETY S., DAHAL R., ZHAO W. P., LIN J. Y. and JIANG H. X., *Appl. Phys. Lett.*, **101** (2012) 171112.
- [17] MUHTADI S., HWANG S., COLEMAN A., ASIF F., LUNEV A., CHANDRASHEKHAR M. V. S. and KHAN A., *Appl. Phys. Lett.*, **110** (2017) 193501.
- [18] KUMAR S., PRATIYUSH A. S., DOLMANAN S. B., TRIPATHY S., MURALIDHARAN R. and NATH D. N., *Appl. Phys. Lett.*, **111** (2017) 251103.
- [19] LEE C. J., WON C. H., LEE J. H., HAHM S. H. and PARK H., *Sensors*, **17** (2017) 1684.
- [20] CHEN X. H., HAN S., LU Y. M., CAO P. J., LIU W. J., ZENG Y. X., JIA F., XU W. Y., LIU X. K. and ZHU D. L., *J. Alloys Compd.*, **747** (2018) 869.
- [21] LI S., ZHANG Y., YANG W., LIU H. and FANG X., *Adv. Mater.*, **32** (2020) 1905443.
- [22] MENDOZA F., MAKAROV V., WEINER B. R. and MORELL G., *Appl. Phys. Lett.*, **107** (2015) 201605.
- [23] XU X., CHEN J., CAI S., LONG Z., ZHANG Y., SU L., HE S., TANG C., LIU P., PENG H. and FANG X., *Adv. Mater.*, **30** (2018) 1803165.
- [24] CALDWELL J. D., AHARONOVICH I., CASSABOIS G., EDGAR J. H., GIL B. and BASOV D. N., *Nat. Rev. Mater.*, **4** (2019) 552.
- [25] VUONG T. Q. P., CASSABOIS G., VALVIN P., JACQUES V., LEE A. VAN DER, ZOBELLI A., WATANABE K., TANIGUCHI T., GIL B., VAN DER LEE A., ZOBELLI A., WATANABE K., TANIGUCHI T. and GIL B., *2D Mater.*, **4** (2016) 011004.
- [26] LAZIĆ S., ESPINHA A., PINILLA YANGUAS S., GIBAJA C., ZAMORA F., ARES P., CHHOWALLA M., PAZ W. S., BURGOS J. J. P., HERNÁNDEZ-MÍNGUEZ A., SANTOS P. V. and VAN DER MEULEN H. P., *Commun. Phys.*, **2** (2019) 113.
- [27] CHEN H., LIU H., ZHANG Z., HU K. and FANG X., *Adv. Mater.*, **28** (2016) 403.
- [28] CASSABOIS G., VALVIN P. and GIL B., *Nat. Photon.*, **10** (2016) 262.
- [29] FERREIRA F., CHAVES A. J., PERES N. M. R. and RIBEIRO R. M., *J. Opt. Soc. Am. B*, **36** (2019) 674.
- [30] WATANABE K., TANIGUCHI T. and KANDA H., *Nat. Mater.*, **3** (2004) 404.
- [31] ZHOU A. F., ALDALBAHI A. and FENG P., *Opt. Mater. Express*, **6** (2016) 3286.
- [32] LIU H., MENG J., ZHANG X., CHEN Y., YIN Z., WANG D., WANG Y., YOU J., GAO M. and JIN P., *Nanoscale*, **10** (2018) 5559.
- [33] WANG Y., MENG J., TIAN Y., CHEN Y., WANG G., YIN Z., JIN P., YOU J., WU J. and ZHANG X., *ACS Appl. Mater. Interfaces*, **12** (2020) 27361.
- [34] HOMOLA J., YEE S. S. and GAUGLITZ G., *Sens. Actuators B: Chem.*, **54** (1999) 3.

- [35] WILLETS K. A. and VAN DUYN R. P., *Annu. Rev. Phys. Chem.*, **58** (2007) 267.
- [36] HUTTER E. and FENDLER J. H., *Adv. Mater.*, **16** (2004) 1685.
- [37] HOMOLA J. and PILARIK M., *Surface Plasmon Resonance (SPR) Sensors* (Springer) 2006, pp. 45–67.
- [38] LI M., CUSHING S. K. and WU N., *Analyst*, **140** (2015) 386.
- [39] CHEN H., SU L., JIANG M. and FANG X., *Adv. Funct. Mater.*, **27** (2017) 1704181.
- [40] SINGH P., *Surface Plasmon Resonance* (Nova Science Publishers, Inc.) 2014.
- [41] GORKUNOV M. V., STURMAN B. I. and PODIVILOV E. V., *EPL*, **110** (2015) 57004.
- [42] SUI M., KUNWAR S., PANDEY P. and LEE J., *Sci. Rep.*, **9** (2019) 1.
- [43] BLABER M. G., ARNOLD M. D., HARRIS N., FORD M. J. and CORTIE M. B., *Phys. B: Condens. Matter*, **394** (2007) 184.
- [44] KNIGHT M. W., LIU L., WANG Y., BROWN L., MUKHERJEE S., KING N. S., EVERITT H. O., NORDLANDER P. and HALAS N. J., *Nano Lett.*, **12** (2012) 6000.
- [45] LIU H., MENG J., ZHANG X., CHEN Y., YIN Z., WANG D., WANG Y., YOU J., GAO M. and JIN P., *Nanoscale*, **10** (2018) 5559.
- [46] DOAN T. C., LI J., LIN J. Y. and JIANG H. X., *AIP Adv.*, **6** (2016) 075213.
- [47] YANG H., WANG L., GAO F., DAI M., HU Y., CHEN H., ZHANG J., QIU Y., JIA D. C., ZHOU Y. and HU P., *Nanotechnology*, **30** (2019) 245706.
- [48] DAHAL R., LI J., MAJETY S., PANTHA B. N., CAO X. K., LIN J. Y. and JIANG H. X., *Appl. Phys. Lett.*, **98** (2011) 211110.
- [49] TIZEI L. H. G., LOURENÇO-MARTINS H., DAS P., WOO S. Y., SCARABELLI L., HANSKE C., LIZ-MARZÁN L. M., WATANABE K., TANIGUCHI T. and KOCIAK M., *Appl. Phys. Lett.*, **113** (2018) 231108.
- [50] ZHANG X., CHEN Y. L., LIU R.-S. and TSAI D. P., *Rep. Prog. Phys.*, **76** (2013) 046401.
- [51] KOWALSKA E., ABE R. and OHTANI B., *Chem. Commun.*, issue No. 2 (2009) 241 (DOI: 10.1039/B815679D).
- [52] NISHIJIMA Y., UENO K., YOKOTA Y., MURAKOSHI K. and MISAWA H., *J. Phys. Chem. Lett.*, **1** (2010) 2031.
- [53] MÜHLSCHLEGEL P., EISLER H. J., MARTIN O. J. F., HECHT B. and POHL D. W., *Science*, **308** (2005) 1607.
- [54] SCHULLER J. A., BARNARD E. S., CAI W., JUN Y. C., WHITE J. S. and BRONGERSMA M. L., *Nat. Mater.*, **9** (2010) 193.
- [55] LIU S., LI M. Y., SU D., YU M., KAN H., LIU H., WANG X. and JIANG S., *ACS Appl. Mater. Interfaces*, **10** (2018) 32516.
- [56] LIU Z., HOU W., PAVASKAR P., AYKOL M. and CRONIN S. B., *Nano Lett.*, **11** (2011) 1111.
- [57] GRIGORCHUK N. I., *EPL*, **97** (2012) 45001.
- [58] MAIER S. A., *Plasmonics: Fundamentals and Applications*, Vol. **677** (Springer, New York) 2004.
- [59] KOHN W. and SHAM L. J., *Phys. Rev.*, **140** (1965) A1133.
- [60] PERDEW J. P., BURKE K. and ERNZERHOF M., *Phys. Rev. Lett.*, **77** (1996) 3865.
- [61] KRESSE G. and FURTHMÜLLER J., *Phys. Rev. B*, **54** (1996) 11169.
- [62] GRIMME S., *J. Comput. Chem.*, **27** (2006) 1787.
- [63] WU X., VANDERBILT D. and HAMANN D. R., *Phys. Rev. B*, **72** (2005) 035105.
- [64] LATURIA A., VAN DE PUT M. L. and VANDENBERGHE W. G., *npj 2D Mater. Appl.*, **2** (2018) 6.
- [65] JOHNSON P. B. and CHRISTY R. W., *Phys. Rev. B*, **6** (1972) 4370.
- [66] RAKIĆ A. D., *Appl. Opt.*, **34** (1995) 4755.
- [67] KNIGHT M. W., KING N. S., LIU L., EVERITT H. O., NORDLANDER P. and HALAS N. J., *ACS Nano*, **8** (2014) 834.
- [68] GAO N., HUANG K., LI J., LI S., YANG X. and KANG J., *Sci. Rep.*, **2** (2012) 816.
- [69] ZHANG W., XU J., YE W., LI Y., QI Z., DAI J., WU Z., CHEN C., YIN J., LI J., JIANG H. and FANG Y., *Appl. Phys. Lett.*, **106** (2015) 021112.
- [70] MATVEEV A. T., PERMYAKOVA E. S., KOVALSKII A. M., LEIBO D., SHCHETININ I. V., MASLAKOV K. I., GOLBERG D. V., SHTANSKY D. V. and KONOPATSKY A. S., *Ceram. Int.*, **46** (2020) 19866.
- [71] KELLY K. L., CORONADO E., ZHAO L. L. and SCHATZ G. C., *J. Phys. Chem. B*, **107** (2003) 668.
- [72] LI X., JORDAN M. B., AYARI T., SUNDARAM S., EL GMILI Y., ALAM S., ALAM M., PATRIARCHE G., VOSS P. L., SALVESTRINI J. P. and OUGAZZADEN A., *Sci. Rep.*, **7** (2017) 786.